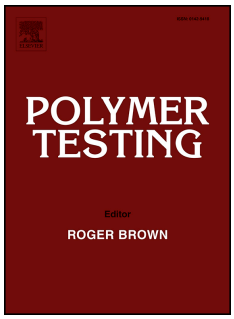

Characterization of direct ink write pure silk fibroin based on alcohol post-treatments

Enric Casanova-Batlle, Antonio J. Guerra, Joaquim Ciurana

PII: S0142-9418(22)00305-1

DOI: https://doi.org/10.1016/j.polymertesting.2022.107784

Reference: POTE 107784

To appear in: *Polymer Testing*

Received Date: 11 July 2022

Revised Date: 5 September 2022

Accepted Date: 9 September 2022

Please cite this article as: E. Casanova-Batlle, A.J. Guerra, J. Ciurana, Characterization of direct ink write pure silk fibroin based on alcohol post-treatments, *Polymer Testing* (2022), doi: https://doi.org/10.1016/j.polymertesting.2022.107784.

Characterization of direct ink write pure silk fibroin based on alcohol post-treatments

Enric Casanova-Batlle[a], Antonio J. Guerra[b], Joaquim Ciurana[a]

[a] Grup de Recerca d'Enginyeria Producte Procès i Producció, Universitat de Girona, Pic de Peguera 15, 17003, Girona, Spain.

[b] EURECAT, Centre Tecnològic de Catalunya, Plaça de la Ciència 2, 08243 Manresa, Spain

* Corresponding:

Email: quim.ciurana@udg.edu

Present address: [a] Grup de Recerca d'Enginyeria Producte Procès i Producció, Universitat de Girona, Pic de Peguera 15, 17003

Keywords

Silk fibroin; Direct ink writing; Post-treatments; Additive manufacturing; Materials engineering

Abstract

Silk fibroin (SF) has been successfully used for medical devices due to its biodegradability with non-toxic end products, high tensile strength and mechanical robustness, but also because of its high flexibility potential. Although natural silk fibers have excellent strength and flexibility, regenerated silk materials generally become brittle in the dry state. For this reason, researchers have studied the effects that manufacturing and post-treatment parameters have on their mechanical properties, but they have also studied the impact on other factors such as biodegradability on the environment. This work presents an optimized process for direct ink write a regenerated SF bioink and its possible post-treatments. A simple method to concentrate the aqueous SF has been reported. The technique was then employed to 3D print test specimens for multiple mechanical analysis to characterize the resulting parameters of the processed silk. The effect of post-treating the material with different processes (no-treatment, immersion in ethanol for 24h, and subsequently immersion in methanol for 30, 60 or 120 min) was explored. The different post-treatments resulted in distinct effects on the silk properties, suggesting that SF molecular structure could be controlled by the post-treatment process. The results showed a transition to phosphate-buffered saline (PBS)-insoluble silk when the silk was treated with alcohols. This resulted in a more brittle material than the untreated group, with a lower strain at break. Nevertheless, the post-treatments enhanced the stability of silk in water, as they reported greater insolubility in PBS than the untreated group. This study characterizes and discusses the mechanical properties of SF processed with a novel additive manufacturing method intended for customization of medical devices.

1. Introduction

Silk fibroin (SF) has been successfully implemented in the biomedical field. Wound healing, drug release or bio-electronics are some of the many applications that SF has been used in the recent years [1]–[3]. This wide range of applicability within the human body is due to its biodegradability with non-toxic end products, high tensile strength and mechanical robustness, but also because of its high flexibility potential [4]. The trend towards customized medical devices makes interesting the ability to 3D print this material to fabricate patient-specific implants [5]. Therefore, a system to 3D print SF opens new opportunities for personalized health care systems. For instance it could be utilized to fabricate bioresorbable cardiovascular stents. Some studies have attempted to manufacture stents through tubular 3D printing with biodegradable materials such as PCL [6]. However, polymeric stents offer bulkier designs as they have weaker mechanical properties than metallic stents. Bigger designs can cause in-stent restenosis [7] and difficulties accessing small vessels [8]. Therefore, the mechanical properties that silk offers could represent a good alternative to address this challenge [9]. Moreover, silk has been assessed *in vivo* in terms of thrombogenicity and vascular cell responses [20]. Hence, cardiovascular applications are a perfectly suitable scenario for this material.

SF has two types of molecular structures, silk I and silk II. Silk I is a metastable structure with α-helix and random coil bonds. Solubility in water and mechanical properties lower than the silk II are the main characteristics of silk I. Type II of silk has a molecular structure in the form of ß-sheet, stronger and more stable bonds. Aforementioned features make it insoluble in water and potentially more resilient to mechanical stress. [10]. These states of SF make it customizable to the type of application required. Controlling the state in which silk fibroin is encountered in the final application has been a case of study in the recent past. The molecular structure of SF could be controlled by various physicochemical processes. The transition of SF to secondary structures has been studied by chemical post-treatments, typically with alcohols. Studies showed that both vaporization and immersion treatments with ethanol (EtOH) and methanol (MeOH) increase the ß-sheet content. Therefore, as the modified structure is more stable, parameters such as glass transition temperature (Tg) and water insolubility also increase [11], [12]. Further, among the alcohols, MeOH is the best precursor for the reaction. Thus, it causes a greater effect on all the listed characteristics, with immersion being the strategy that has the greatest impact [11]. Nevertheless, EtOH post-treatments also induce silk II conformations and has been employed for biomedical applications [13], [14]. Finally, glutaraldehyde has also been used as a chemical crosslinker to increase the stability of the silk molecular structure, thus promoting the formation of the ß-sheet structures [15].

Additionally, physical parameters could be controlled during the post-treatment such as the temperature, humidity or pH to influence both the molecular structure and properties of the silk [16]. Wang *et al.* tested the relationship between temperature, humidity and silk molecular structure during the water annealing process and found that the higher the humidity and the temperature the higher the increase in the silk II content [17]. Furthermore, the water content entangled within the chains of the silk fibroin could act as plasticizers of the material [18], [19]. In this way, a flexible and stable silk structure was achieved. Finally, to promote the reaction of silk I to silk II while maintaining the flexible properties of the silk, mechanical stretching of the silk in the wet state could be performed. The SF post-treated with this technique had an increase in the structural formation of the ß-sheet maintaining higher levels of elasticity than the regenerated silk post-treated with MeOH reagent [19].

3D printing or Direct Ink Writing (DIW) SF requires an ink with a certain viscosity which in the past has been achieved with the addition of other reagents, such as laponite, gelatin, or hyaluronic acid [21], [22]. Alternative methods can be found in literature, including crystallization enhancement with MeOH treatment or photo-crosslinking [23], [24]. However, the addition of these compounds hinders the printing process. Our previous study validated the feasibility of printing pure SF at high concentrations, ensuring print quality with 500 µm wide filaments [25]. The system was based on the gelation of high concentrated SF by heating the nozzle and the deposition bed which catalyzed the evaporation of water from the solution. Nevertheless, the fabricated material showed unstable mechanical properties, as they were influenced by the ambient humidity. A high silk I content was found in the Fourier transform infrared (FTIR) test, so it was hypothesized that the affinity for water of this structure varied the mechanical properties.

For stent application, the silk should degrade within the body gradually after being completely dissolved. In order to tune the rate of silk degradation the present study proposes a partial transition from silk I to silk II with the post-treatment of alcohols, which are catalysts for this structural transition [11]. The hypothesis was that increasing the silk II content of the printed structures would provide more stability in aqueous solutions and increased and more stable mechanical properties of the printed material. More specifically, it was intended to achieve different printed structures with different silk II contents by treating them with different exposure times in MeOH. In order to manufacture test specimens made of concentrated pure SF, the present study analyzes for the first time (to the authors' knowledge) the possibility of concentrating SF up to 56.69 - 60.09 % (w/w) to increase its viscosity and printing it via DIW. Thus, meeting the rheological properties to make the DIW process of the bioink feasible, so that the bioink did not scatter after its deposition.

Therefore, this study has evaluated the mechanical properties of silk, as well as its molecular structure and degradation rate to estimate its potential in medical device customization. The objective is to find a successful procedure to post-treat SF so that its mechanical properties are consistent as well as its degradation rates.

2. Methodology

2.1. Preparation of the ink

Bombyx mori cocoons were kindly supplied by the association to preserve the silk worm in Spain (AERCEGSA) and the *Granja de la seda* institution for the development of the sericulture. Then, the SF was extracted according to the method previously described [26]. Briefly, to remove sericin from the silk, cocoons were immersed in 0.08 w/v % Na_2CO_3 (Sigma Aldrich, USA) solution at boiling temperature for 30 min. Then, they were washed with distilled water, and dried at room temperature overnight. Dried SF fibers were then dissolved in 9.3 M LiBr (Sigma Aldrich, USA) solution and dialyzed against MiliQ water using a SnakeSkin™ dialysis membrane of 3.5K MWCO (Live Technologies, USA) for 2 days at 4 °C to remove the salt. The aqueous solution was subsequently filtered with Miracloth (Merck, USA). The resulting SF solution was approximately 5 – 7 w/w %. This aqueous solution was then dialyzed against 20 w/v % polyethylene glycol (PEG) (8000 g/mol , Sigma Aldrich, USA), 1 M $CaCl_2$ (Anhydrous > 93 %, Sigma Aldrich, USA) and 50 mM Trizma® base (Sigma Aldrich, USA) at 4 ºC using the SnakeSkinTM dialysis membrane of 3.5K MWCO. The solution was adjusted at pH =8. After 24 h the concentrated SF solution was 56.69 - 60.09 w/w %. It was removed from the dialysis membrane and stored at 4 °C before use. All the concentrations of SF were determined by comparing the weight of 0.5 mL of solution to the mass of silk after drying at 70 °C for 12 h.

2.2. Printing the test specimens

Tensile tests specimens were printed using a three-axis micropositioning stage controlled by customized software (gcode, Processing) following the ASTM D882-02 norm. The concentrated SF solution was housed in a discardit II 5 mL syringe (BD, USA) mounted on the ink extruder which was connected with a PVC tube (1.6 mm inner diameter and 200 mm length) to an x-y-z stage. The SF ink was extruded through a G25 gauge needle (Nordson, USA) onto a crystal bed with a flat surface which had stack a polypropylene adhesive tape. The bed was previously heated at 45 ºC and maintained during the entire process. The rotation of the motor ensured a constant deposition speed of 10.9 µL/mm. As the ink exited the nozzle, a continuous filament was printed. It retained the deposited shape due to ink viscosity and the reduced gelation time resulting of the applied heat.

The shape of the test specimen consisted of depositing 80 mm lines 0.5 mm apart, with a total of 30 lines per test specimen. At the end of each line the piston was retracted 1.1 mm to release residual pressure in the system and ensure a constant impression. The displacement speed of the nozzle was 500 mm/min. All test specimens were dried 48 h at 25 ºC and 70 % of relative humidity.

2.3. Post-treatments

Five different post-treatments were conducted to characterize the mechanical properties of the deposited SF (Figure 1):

Intermittent heat and humidity (NT): The tests specimens were subjected to 5 min of dry heat at 75 ºC and, cooled at 25 ºC and 70 % of humidity for 1 hour. Then, the test pieces were subjected to a humidity test with a dry heat of 75 ºC and a dew point of 65 ºC during 15 min. At that point they were disassembled from the adhesive tape and, dried under the hood. Therefore, this samples were no treated (NT) with any chemical reagent.

EtOH: The tests specimens were immersed with EtOH 96 % for 24 hours.

Methanol (Me30 – Me60 – Me120): The tests specimens were immersed with EtOH 24 hours. Then, they were dried under the hood and immersed with MeOH ≥ 99.8 % (labkem, Spain) for 30 min, 60 min or 120 min.

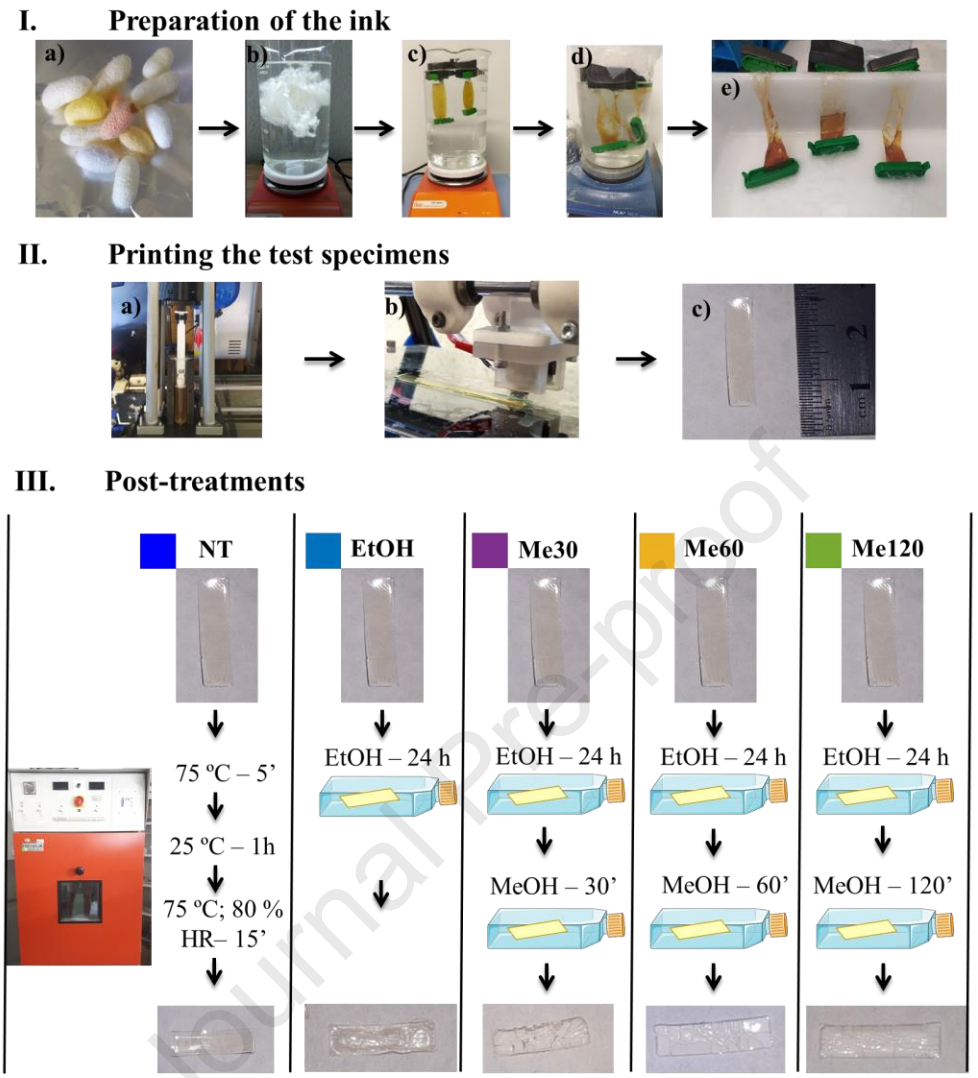

Figure 1 Diagram of the methodology employed throughout the different post-treatments for the acquisition of the test specimens. I-a) Raw cocoons. I-b) SF washed after boiling step. I-c) Dialysis against MiliQ water. I-d) Dialysis against 20 w/v % PEG. I-e) Resulting SF ink. II-a) SF solution housed in a syringe. II-b) Printing test specimens. II-c) Resulting test specimens. III) Post-treatment scheme of the experimental specimens.

2.4. Characterization

To comply with the ASTM D882-02 standards 5 replicates were fabricated for each of the five described post-treatments. Each one of them was subjected to the following characterization tests.

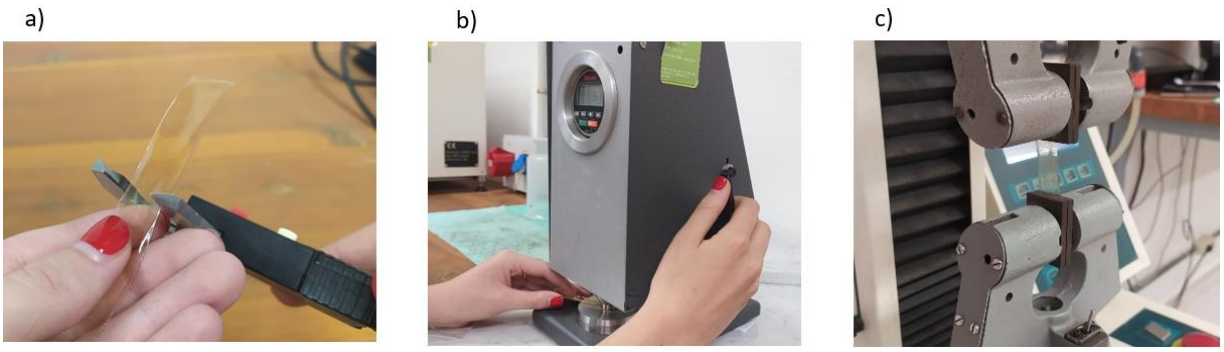

Figure 2 Measurements taken during the tensile test. a) Width of specimen. b) Thickness of specimen. c) ASTM D882-02 tensile test.

Mechanical properties of the DIW SF were evaluated using tensile test under control conditions of 50 % relative humidity at room temperature, Figure 2. The printed rectangle specimens of SF (80 x 15 mm) were tested under tensile stress, without extensometer, in a Hounsfield Universal Testing Machine (Shakopee, USA) equipped with a load cell of 2.5 kN. These parameters were set according to ASTM D 882-02 standard specifications. Data of five specimens were collected to obtain the statistical standard deviation for each sample.

2.5. Fourier Transform Infrared (FTIR) Spectroscopy

After testing, the test specimens were collected. IR spectra (4000–350 cm-1) was taken in an infrared spectrometer (Alpha Bruker FT-IR, USA) using a single reflection ATR system.

2.6. Degradation Assay

Test specimens of 20 x 5 mm were fabricated. The samples were weighed by a Sartorius ED224S analytical balance (Sartorius, Göttingen, Germany), and transferred to non-adherent cell culture 12-well plates (Sarstedt, Germany). 2 mL of PBS was added into each well and kept in the incubator for 15 min, 30 min, 4 hours, 1 day or 5 days, Figure 3-a. Water absorption and weight loss were evaluated by weighing the samples on a weighting scale(Mettler Toledo Sartorius 2MP Scale, USA), taking into account the sample's original weight after the post-treatment process (W_0), weight of the wet/dry sample (w/w), and residual weight after degradation once it had been completely dried (W_d) in an oven for 24 h at 75 ºC. The water absorption rate, W_a%, was evaluated with equation 1:

$$W_a\% = \frac{W_w - W_d}{W_d} * 100 \qquad \text{Eq. 1}$$

Weight loss percentage, $W_L\%$, was estimated using equation 2:

$$W_L\% = \frac{W_O - W_d}{W_O} * 100 \qquad \text{Eq. 2}$$

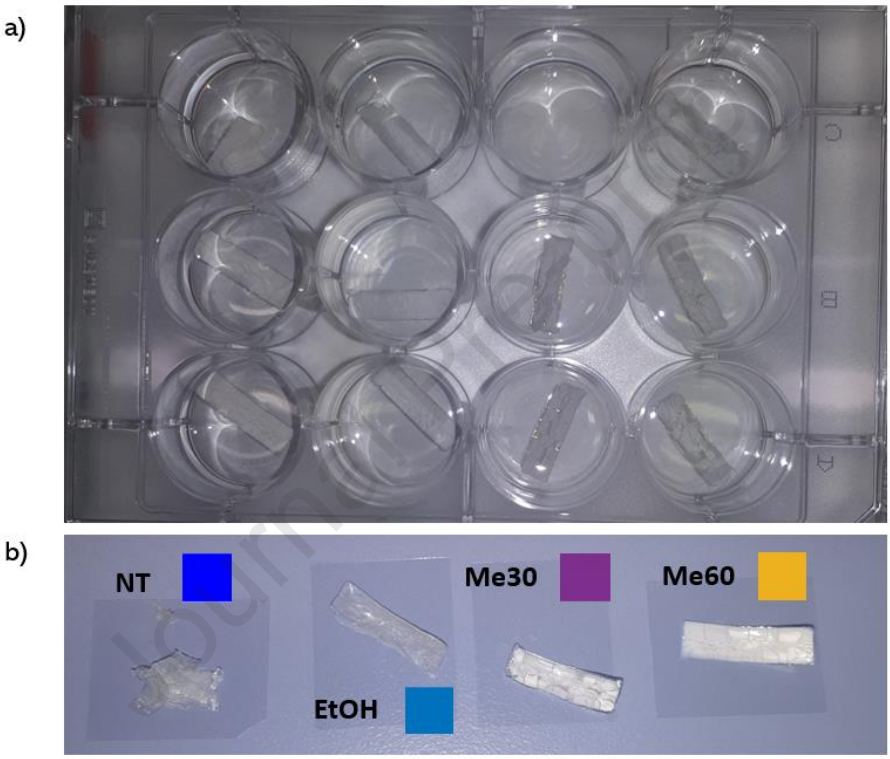

Figure 3 a) Degradation test. A sample was placed in each well and was filled with 2 mL of PBS. b) Representative image of the specimens after 1 hour of degradation.

2.7. Dynamic Mechanic Analysis (DMA)

A Mettler Toledo DMA/SDTA 861 equipped with dual cantilever tools was used to perform the DMA analysis. The test was run with a preload of 1 N and a frequency of 1 Hz. The samples (N=2) were heated from 0 to 230 ºC or specimen rupture at 5 ºC/min in an air atmosphere.

2.8. Differential scanning Calorimetry (DSC)

The thermal properties of the obtained specimens were assessed by means of differential scanning calorimetry using a TA Instruments DSC Q2000 in order to evaluate the influence of the post-treatments on the thermal transitions. Scans were run from 30 to 305 ◦C at a heating rate of 10 ◦C/min. The test was performed in an inert atmosphere with a nitrogen flow rate of 50 ml/min.

2.9. Thermal gravimetric analysis (TGA)

A Mettler-Toledo TGA/DSC 1 thermobalance was used to analyze the weight loss while heating. The samples were heated from 30 to 700 ◦C with a heating rate of 10 ◦C/min. The test was performed in an inert atmosphere with a nitrogen flow rate of 50 ml/min.

2.10. SDS PAGE – Molecular weight (M_w) determination

The M_W of fibroin was estimated using SDS PAGE Electrophoresis as follows: 10 µg of SF was added into a 1: 1 buffer sample containing reducing agent and heated at 85◦C for 30 seconds. Then 20µl of the sample were loaded on 10% (w/v) acrylamide gel. Electrophoresis was carried out using the Mini-PROTEAN Tetra Cell-BIO RAD. After electrophoresis, the gel was stained with Coomassie blue (ThermoFischer, USA).

2.11. Viscosity

The viscosity of the ink was measured with a Myr Serie VR 3000 rotatory viscometer (Viscotech Hispania S.L., Spain).

3. RESULTS

3.1. M_W of regenerated SF before DIW

A parameter that impacts on the mechanical and physical parameters such as the storage modulus (E') or the degradation rate of the regenerated SF is the M_w. For this reason, this parameter was characterized at the beginning of the tests.

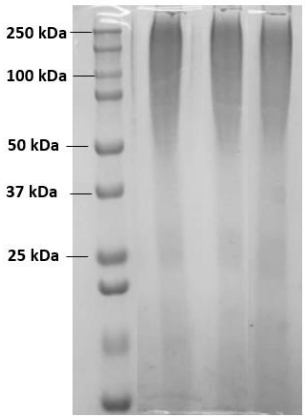

Figure 4 Acrylamide gel loaded with 10µg of fibroin after electrophoresis (N=3)

The M_W of the SF chains found in the material before printing were in the range between 250 kDa and 50 kDa and weak bands were observed at 25 kDa. It is worth noting that these findings are in concordance with the current literature. Silk degummed during 30 min in a concentration of 0.05 w/v% Na_2CO_3, as approximately conducted in this work (0.08 w/v %), should exhibit a broad distribution centered at 100 kDa [27], [28]. Therefore, a small degradation of the SF chains occurred due to heat and alkaline hydrolysis under the Na_2CO_3 action.

3.2. Determination of molecular structure

In order to determine the silk I and silk II structure, the FTIR spectra was obtained in the spectral region 350-4000 cm^{-1}. The bands at 1230, 1540, and 1640 cm^{-1} are assigned to α-helix/random coil conformation (related to silk I), while the bands at 1261, 1620, and 1696 cm^{-1} are assigned to the ß-sheet structures (silk II) [29]–[31]. Therefore, the absorption in these bands indicated the molecular structure of the ink and it was used to evaluate the following outcomes of the material.

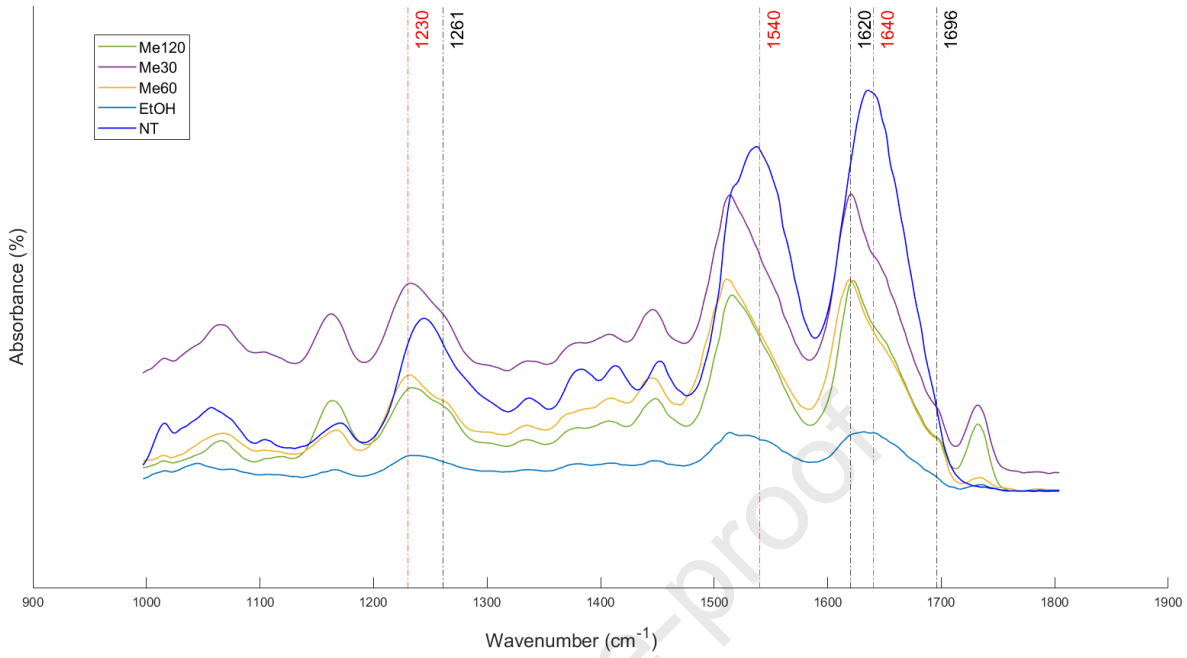

Figure 5 FTIR spectra of 3D printed SF tensile specimens' groups. The red-dashed vertical lines corresponds to the absorption bands associated to random coil and α-helix conformation. The black-dashed vertical lines corresponds to the absorption bands characteristic to the ß-structure.

The test specimens treated with MeOH presented silk II characteristic peaks. Specifically, the peak at the 1620 cm^{-1} wavenumber was observed in all the MeOH-treated test specimens. In contrast, NT silk displayed peaks at the absorbance bands corresponding to silk I (Figure 5). For instance, it presented a peak shifted at 1640 cm^{-1} which corresponded to silk I. In between, EtOH-treated silk exhibited a combination of the two different types. These samples showed an absorbance level equally high between these frequencies (1620-1640 cm^{-1}). This might indicate that the silk treated with this method contained both silk I/II conformations.

Moreover, a curve deformation was observed in the 1261 and 1696 cm^{-1} absorption bands corresponding to the ß-sheet structure, supporting the presence of silk II molecular structure within the MeOH post-treated silk. These signal perturbations were more pronounced the higher the exposure to the MeOH reagent. Interestingly, the reported results for Me60 and Me120 showed similar outcomes, whereby there might be a threshold at which all silk shifted to its type II structure and no further changes were found in the FTIR spectra. This trend change was hardly observed in the group of specimens treated with EtOH.

Finally, all groups presented absorbance peaks corresponding at the silk I molecular structure, indicating that the α-helix conformation was present in all the silk subtypes. A remarkable absorbance on the 1230 cm^{-1} peak could be observed throughout all the post-treated groups, indicating that these groups also presented silk I molecular structure. The NT group also presented α-helix specific point at 1540 cm^{-1}.

3.3. Thermal analysis

Table 1: Parameters of interest for the description of the thermal tests

	EtOH	Me30'	Me60'	Me120'
TGA				
Water content (%)	14.86	11.15	10.33	10.25
T_{wl} (ºC)	216.00	200.50	189.67	211.33
T_{onset} (ºC)	297.11	283.20	278.39	276.88
DSC				
T_t (ºC)	208.02	170.95	193.96	185.82
ΔH_{wl} (J/g)	380.5	256.6	325.5	305.9
$T_{max\ wl}$ (ºC)	89.12	78.38	98.13	92.34

Thermal assays were performed to the post-processed materials to describe their behavior with an increasing temperature. Two events were described with the TGA and DSC tests, the water loss event and the SF degradation event, Figure 6. The water loss event indicated the water content of the initial material (Table 1). Furthermore, the temperature at which the SF began its degradation was calculated. To calculate the water content of the samples, it was hypothesized that the water loss event comprised the temperatures from the beginning of the test to the point on the curve depicting the lowest slope, temperature of water loss (T_{wl}), before entering the fibroin degradation event. Thus, the mass lost up to this point was considered water. Figure 6-a shows that NT group had the highest water

content (18.3 %), among all conditions. Also, it was highlighted that silk post-treated only with EtOH presented a higher water content than the MeOH treated groups.

The temperature at which fibroin began its degradation was defined as the onset temperature (T_{onset}). This was calculated at intersection point between the tangent line to the baseline before mass loss and the tangent line to the inflection point during mass loss. The silk types treated with longer exposures to MeOH degraded at lower temperatures than the subgroup only treated with EtOH (Figure 6).

a) b)

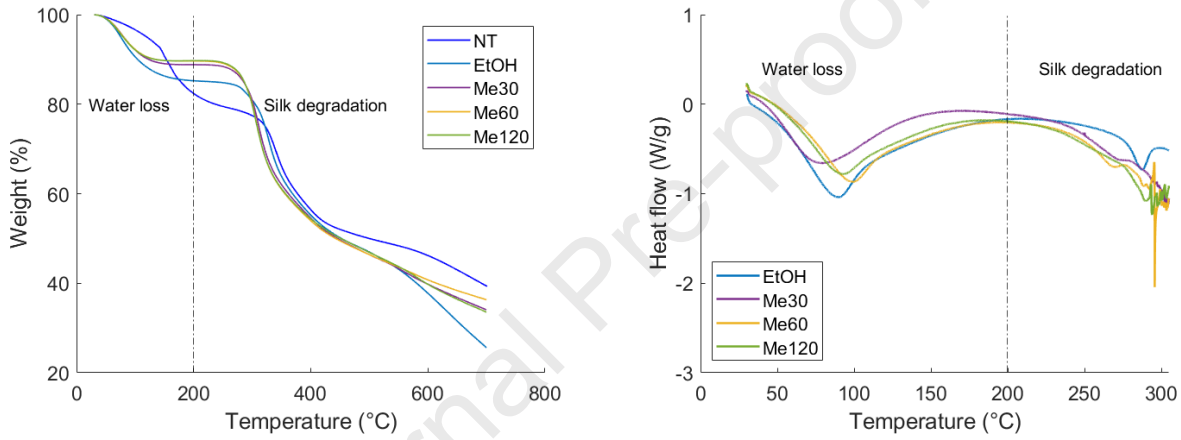

Figure 6 Thermal behavior of DIW SF. a) Thermal gravimetric analysis (TGA) of 5 mg of the sample treated with the different post-treatments. b) Heat flow vs temperature during Differential Scanning Calorimetry (DSC) of regenerated SF.

The DSC test confirmed the events seen by the TGA assay, Figure 6-b. For instance, the water loss event was reported as an endothermic reaction (ΔH_{wl}). Table 1 reports the temperature at which the endothermic reaction's derivative reached its maximum absolute slope ($T_{max\ wl}$). The temperature of transition (T_t) between the water loss event and the silk degradation was described as the smaller slope baseline, calculated with the derivative. As described with the TGA test the content of water was higher at the samples only treated with EtOH, since its enthalpy score during the water loss event was described as the highest throughout the studied groups.

3.4. Mechanical properties

Results of the tensile test according to the ASTM D882-02 norm can be encountered in Table 2. Data revealed a reduction of the elasticity of the material under post-treatments with alcohols and a transition to a brittle fracture. On one hand, the silk treated only with EtOH maintained its structure and could be tested, showing a 54.00 % reduction in Young's modulus (E) and 51.70 % reduction in the ultimate tensile strength (UTS) compared to NT silk. On the other hand, MeOH treated tensile specimens were subjected to morphological alterations, Figure 71. This event caused the specimens to lose their consistency. As a direct consequence, the material performed poorly in terms of tensile strength, with an average UTS 74.55 % lower, in the best case scenario, Figure 7. The test specimens were very fragile due to the folds, which sometimes cracked before they were tested during placement.

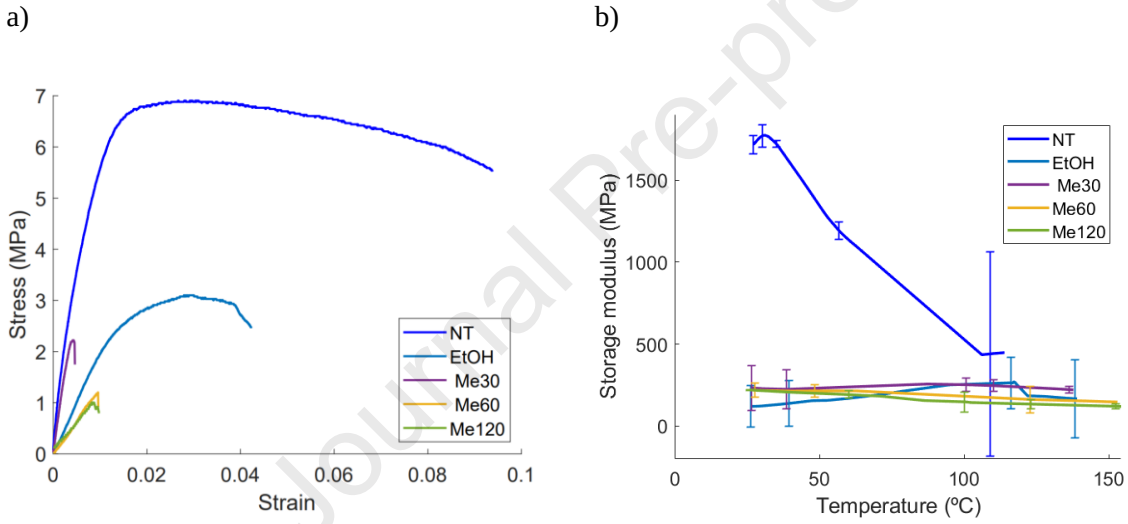

Figure 7 Data of mechanic analysis. a) Represents the raw data of a representative tensile test replicate for each post-treatment. b) Depicts the mean values and standard deviation (SD) of the storage modulus with their respective temperature extracted from the DMA test (N=2).

Figure 7-b presents the storage modulus (E') for each respective temperature. Therefore, the behavior of the E' with increasing temperature. Consistently, the E' at room temperature had similar values to the E. Furthermore, the data depicted a stiffening of the material during the water loss event as an increase in the E'. This subtle increase in the E' with increasing temperature was mainly observed with the NT and EtOH-treated silk subgroup. This trend appeared to be less pronounced, but was still present in the group treated with Me30 and was no present for the Me60 and Me120 subgroups. At the end of this event, the test specimens decreased their E' coinciding with the degradation

phase, except for the NT subgroup which started earlier. Finally, the exposure time with MeOH in post-treatment seemed to show a reduction of the E'. This was reflected in Figure 7-b, where, on average, the samples treated with Me30 showed a higher modulus than those treated with Me60 and these with Me120, respectively.

It should be noted that, although the DMA is not described as a destructive test, since the material is subjected to small stresses to study the elastic behavior, some of the samples collapsed during the test. This would explain, for instance, the high SD exhibited by the EtOH group at 139.1 °C, as a breakage of the test piece occurred. Similarly, the test pieces of the Me60 and the NT group all split. For this reason, only data up to this breakage temperature were presented. These events were evidence of the fragility of the regenerated SF material.

Table 2: Mechanical properties obtained from tensile test under the ASTM D882-02 standards. Last row depicts the storage modulus at room temperature of the DMA test.

Post treatments	**No treated**	**EtOH**	**30'**	**60'**	**120'**
Young's Modulus (MPa)	637 ± 300	293 ± 151	354± 298	363 ± 320	286 ± 178
Ultimate stress (MPa)	8.84 ± 3.73	4.27 ± 2.68	0.98 ± 1.08	2.25 ± 2.33	1.83 ± 1.57
Yield point (MPa)	8.74 ± 3.82	3.69 ± 2.88	0.82 ± 1.16	2.16 ± 2.40	0.46 ± 0.37
Elongation at Break (%)	5.87 ± 2.81	2.56 ± 0.96	2.89 ± 2.42	1.70 ± 1.59	1.01 ± 0.18
E' at r.t. (MPa)	1697.3 ± 39	132.54 ± 96	225.34 ± 86	214.66 ± 27	210.64 ± 1

3.5. Solubility and degradation in PBS

The degradation assay confirmed the hypothesis provided by the literature on the documented molecular structure of the silk [10], [32]. A fast degradation of the samples was observed in the NT silk. This is in agreement with the literature, since more peaks were found in the FTIR curve in the NT group, corresponding to water-soluble silk I. Moreover, the present study offers for the first time the possibility of concentrating SF to high concentrations without gelation. The resulting NT degradation sample presented a high content of silk I. When the specimen was immersed

in PBS, it was partially redissolved, as if it were a lower % w/w solution. Only one replicate showed weak resistance to degradation in water, represented in the SD of Figure 8-a of this group.

Furthermore, the degradation assay confirmed the presence of the coexistence of both types of silk especially in the EtOH specimens. The degradation of the EtOH samples showed a lower early degradation than NT silk in contact with PBS. However, its degradation was faster than the MeOH-treated samples (Figure 8-a). EtOH experienced a mean W_L of 41.72 % of the W_o one hour from the beginning of the test. While for Me30, Me60 and Me120, a 10.02, 9.79 and 6.79 % were described respectively. Thus, the MeOH treated samples depicted the lowest degradation rates. As observed from the FTIR results, the MeOH subgroups exhibited a response corresponding to a high content of water-insoluble silk structure II.

a) b)

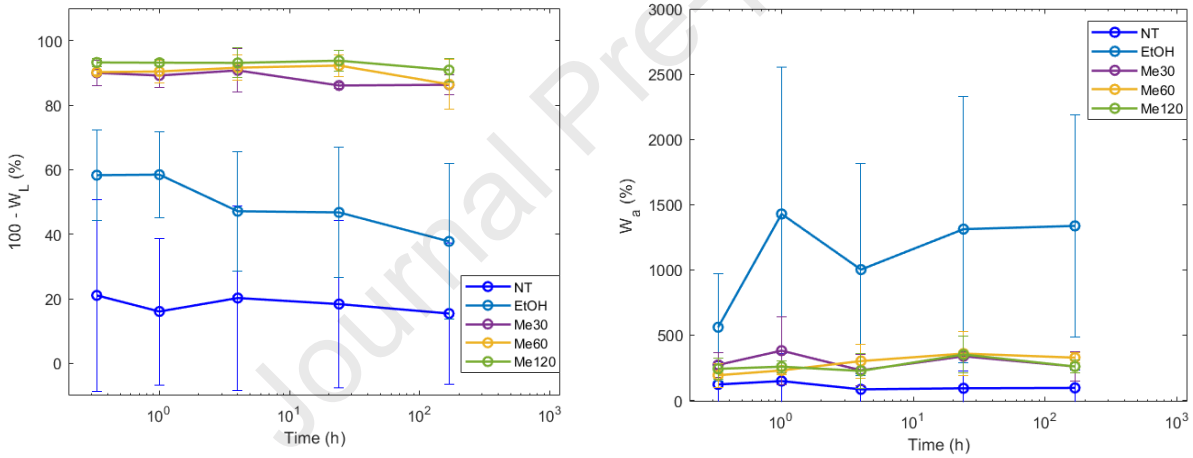

Figure 8 Representation of the degradation test data. a) The percentage of degradation of the specimen after 20', 1h, 4h, 24h and 7 days with their corresponding SD. b) The water absorption after the selected times and SD.

Finally, although W_a had high SD values, they represent a similar trend than W_L. The NT samples had more affinity to water due to their molecular structure. Nevertheless, as most of the NT samples dissolved during the experimental test W_a was equal to 0. That is why, NT showed the lowest values compared to the other groups, Figure 8-b. The EtOH samples presented the highest W_a values. As indicated by the W_L test, they were partially hydrosoluble as opposed to the samples treated with MeOH that were insoluble in water.

4. DISCUSSION

The purpose of the study of silk post-treatments was to obtain a versatile material that can be customized according to the intended biomedical application. The main technical problem in 3D printing pure SF was to concentrate the silk into an ink viscous enough to maintain the shape after deposition. Commonly, silk was concentrated by PEG ($M_W \geq$ 20000 Da) solutions [33]. For example, Ghosh *et al.* attempted to concentrate silk to 28-30 w/v % to DIW. However, in their study they needed a MeOH reservoir to print the ink to enhance a rapid coagulation of the silk, as it was essential to maintain the silk deposited morphology [23]. Nevertheless, this study overcame this hurdle by increasing the pH of the PEG solution. Studies have demonstrated that the SF greatly decreases its gelation time in basic pH mediums [34]. Therefore, in this work, gelation of the SF during concentration was avoided by adjusting the pH of the PEG solution to 8. This novel approach has yielded concentrations (56.69 - 60.09 % w/w) of SF with a viscosity within the range of 1490 ± 370 mPa·s to be printed via DIW while avoiding gelation of the material.

4.1. Silk as a tunable material

The M_W is a key parameter as it affects the degradation rate and mechanical properties. The M_W could be tuned by altering the degumming time or the Na_2CO_3 concentration. The longer the degumming step or the higher the Na_2CO_3 concentration, the lower the M_w would be [35]. Therefore, the ability to control this feature adds another customizable characteristic in the development of potential medical devices made from silk. The 3D printed applications would not only be unique in morphology, but they could also be designed for a specific M_w. The higher the M_w of the SF the higher the mechanical properties, such as the UTS, and the longer the time required for its complete degradation [36]. Therefore, it could be considered as a 4^{th} dimension over which the additive manufacturing system has control.

4.2. Temperature effect

Both thermal tests (DSC and TGA) have defined the same events in the 3D printed silk in a test with increasing temperature. The first event was encountered in the span of temperatures ranging from the start of the test and T_{wl}. TGA and DSC tests described the weight loss related to the absorbed water. [37]. The EtOH subgroup presented a higher water content than the groups treated with MeOH. Moreover, the results seemed to follow a trend between the exposure time to MeOH and the water absorbed by the material, since the longer the exposition to MeOH treatment, the lower the water content was. This is consistent with MeOH inducing the molecular structure silk II, which is

hydrophobic, whereas silk I is a hydrated structure. The second event describes bond cleavage and degradation of the silk, which appeared to occur at higher temperatures for the EtOH-treated silk than for the MeOH-treated subgroups.

The literature also describes two other events that can be found in the DSC test as the T_g and the silk I to silk II transition [38]. However, T_g was not visible in the results of this study. This event should be found around 180 ºC, which in the presented results the test is still depicting the endothermic reaction of water loss. Therefore, as this event has a greater influence on the enthalpy score of the DSC curve, it could be masking T_g. Reducing the rate at which the test temperature increases would be a solution to further investigate this issue. Finally, the enthalpy change corresponding to the transition from silk I to silk II was not met, possibly because the transition from silk I to silk II was induced in the post-treatments prior to the test. Hence, most of the silk had started the trial with the ß-sheet structure. Therefore, the possible content which remained in silk I structure was not sufficient to stand out this reaction, as this event was also not very prominent in the test results [38].

4.3. Mechanical characterization

The treatment of silk with alcohols is known to increase its crystallinity, mechanical properties and water stability [39]. Nevertheless, although researches have attempted to achieve flexible regenerated SF films, silk becomes brittle after treatment with alcohol-based reagents [19]. This study endeavored to investigate the effects of these post-treatments on SF printed via DIW. The results found describe a trend that is opposite to what was expected, as an increase in E and UTS was hypothesized based on the literature [39]. However, what was observed was a decrease in E modulus the longer the exposure with alcohols compared to untreated fibroin. Specifically, a large reduction of about half of the E modulus was observed in the EtOH-treated subgroup. Furthermore, the MeOH-treated groups exhibited an order of magnitude reduction in the UTS feature compared to NT silk. These unexpected results could be explained by the change of molecular structure during the post-treatment technics. Test specimens bent once treated with alcohols, especially in contact with MeOH (Figure 1). These molecular changes generated morphology alterations. These pleats may have caused stress concentration points in the test specimen that led to earlier fragile rupture. In addition, treatments with alcohols induced a more brittle material, as expected and observed by the strain at break [39], [40]. This lack of flexibility aggravated the stress concentration, since the slightest failure of any of the folds resulted in the rupture of the test specimen. For this reason, this reduction of the E modulus and UTS might be

observed instead of an increase. These folds were not observed in other studies, such as Kaewpirom *et al.* film study, as they mixed the alcohols with the blend and then it was let dry [39].

Moreover, this work has 3D printed the test specimens. The addition of subsequent filaments to produce the desired structure has a lower ability to bond the material than other methods such as injection molds [41]. Therefore, each of these filament bonds can create a defect or a point that causes a stress concentration point. It is for this reason that 3D printed SF like other materials after being 3D printed exhibit a reduction in mechanical properties compared to those that have been manufactured in molds.

4.4. Degradation

The degradation test in PBS showed differences in the degradation of the silk samples according to their post-treatment. An early degradation of silk I of the samples at the beginning of the test was described, as a large percentage of the weight was lost during this phase of the experiment in all the groups. Nevertheless, the NT silk presented a higher soluble silk content than the rest of the subtypes, as hypothesized by the FTIR test. Therefore, a higher W_L was represented in this group (W_L = 78.96 %, 20 minutes). Then, a constant degradation rate was observed. Moreover, all groups described the same behavior; a fast W_L, corresponding to the dissolution of silk type I, on PBS solution. Followed by a constant degradation rate of the remaining structure. However, the alcohol-treated samples presented a lower proportion of silk I than the NT samples, as they were exposed to reagents which catalyzed the ß-sheet structure. This fact shows that the longer the exposure to these treatments after DIW of the silk the higher the water insolubility was. However, the exposures at MeOH of 60 and 120 minutes did not present changes in this parameter. Therefore, there could be a threshold at which leaving the reagent for longer does not catalyze more silk II structure in the samples. This is in agreement with the results of the molecular structure reported by FTIR, where almost no changes were observed between the Me60 and Me120 spectra.

4.5. DIW silk perspectives in the biomedical field

Silk has already proven to be a potentially successful material to be in contact with living tissue, in cell culture or used in biomedical applications. Furthermore, there is a growing tendency in the biomedical field towards the personalization of both medical devices and treatments to treat diseases. This work brings these two concepts together and attempted to bring SF closer to the customization of these applications. In addition to providing the vast potential of 3D printing with regenerated SF, this work has investigated the possibility of controlling other process parameters

to maximize customization. Silk has already demonstrated its efficacy in cardiovascular biomedical applications [20]. Therefore, this system offers the potential to fabricate customized silk-based cardiovascular stents, such as those proposed by Guerra *et al.* [6]. In addition, silk has already been used for drug delivery applications [42]. This system would also allow the customization of the geometry, which in turn allows a more localized release as well as the control of its degradation time. These are merely a small fraction of the many examples that this system potentially offers and is capable of producing, with their respective optimizations.

5. CONCLUSIONS

This work presents for the first time a system to 3D print a highly concentrated SF ink using the DIW technique on a flat polypropylene surface. For this purpose, the silk has been concentrated to obtain a paste viscous enough to maintain its shape once deposited on the bed. In addition, the possibility of obtaining different properties of the final material by means of five different post-treatments was studied. We were able to describe and characterize a transition from silk I to silk II due to post-treatments, although mechanical properties of the final product did not improve with respect to the untreated fibroin. Post-treatment with MeOH did not provide satisfactory results, as it alters the morphology of the 3D printed structure. Nevertheless, the post-treatment with EtOH could be a good compromise between acceptable mechanical properties and a transition to a hydrophobic material. Further optimization of this system could lead to medical devices with great potential and personalization in 4 dimensions.

ACKNOWLEDGEMENTS

The authors gratefully acknowledge the support of the Generalitat de Catalunya through the project (BASE3D 001-P-001646) which is co-financed by the European Union Regional Development Fund under the ERDF Operational Program of Catalonia 2014-2020 with a grant of 50% of the total eligible cost. The authors would also like to thank the Generalitat de Catalunya and the European Union for the predoctoral grant FI AGUR 2021FI_B 00363. Finally, special gratitude to *La granja de la seda* and AERCEGSA for the supply of high quality silk cocoons.

REFERENCES

[1] W. Zhang *et al.*, “Silk Fibroin Biomaterial Shows Safe and Effective Wound Healing in Animal Models and a Randomized Controlled Clinical Trial,” *Adv. Healthc. Mater.*, vol. 6, no. 10, p. 1700121, May 2017.

[2] D.-H. Kim *et al.*, “Dissolvable films of silk fibroin for ultrathin conformal bio-integrated electronics,” *Nat.*

Mater. 2010 96, vol. 9, no. 6, pp. 511–517, Apr. 2010.

[3] X. Wang, X. Hu, A. Daley, O. Rabotyagova, P. Cebe, and D. L. Kaplan, "Nanolayer biomaterial coatings of silk fibroin for controlled release," *J. Control. Release*, vol. 121, no. 3, pp. 190–199, Aug. 2007.

[4] C. Li *et al.*, "Design of biodegradable, implantable devices towards clinical translation," *Nature Reviews Materials*, vol. 5, no. 1. Nature Research, pp. 61–81, 01-Jan-2020.

[5] M. J. Rodriguez, T. A. Dixon, E. Cohen, W. Huang, F. G. Omenetto, and D. L. Kaplan, "3D freeform printing of silk fibroin," *Acta Biomater.*, vol. 71, pp. 379–387, Apr. 2018.

[6] A. J. Guerra and J. Ciurana, "Three-Dimensional Tubular Printing of Bioabsorbable Stents: The Effects Process Parameters Have on In Vitro Degradation," *https://home.liebertpub.com/3dp*, vol. 6, no. 1, pp. 50–56, Feb. 2019.

[7] R. He, L. Zhao, V. V. Silberschmidt, and Y. Liu, "Mechanistic evaluation of long-term in-stent restenosis based on models of tissue damage and growth," *Biomech. Model. Mechanobiol.*, vol. 19, no. 5, pp. 1425–1446, Oct. 2020.

[8] D. Hoare, A. Bussooa, S. Neale, N. Mirzai, and J. Mercer, "The Future of Cardiovascular Stents: Bioresorbable and Integrated Biosensor Technology," *Adv. Sci.*, vol. 6, no. 20, p. 1900856, Oct. 2019.

[9] D. N. Rockwood, R. C. Preda, T. Yücel, X. Wang, M. L. Lovett, and D. L. Kaplan, "Materials fabrication from Bombyx mori silk fibroin," *Nat. Protoc.*, vol. 6, no. 10, pp. 1612–1631, Oct. 2011.

[10] M. A. de Moraes, G. M. Nogueira, R. F. Weska, and M. M. Beppu, "Preparation and Characterization of Insoluble Silk Fibroin/Chitosan Blend Films," *Polym. 2010, Vol. 2, Pages 719-727*, vol. 2, no. 4, pp. 719–727, Dec. 2010.

[11] M. Puerta, M. S. Peresin, and A. Restrepo-Osorio, "Effects of Chemical Post-treatments on Structural and Physicochemical Properties of Silk Fibroin Films Obtained From Silk Fibrous Waste," *Front. Bioeng. Biotechnol.*, vol. 8, p. 1355, Dec. 2020.

[12] H.-Y. Wang and Y.-Q. Zhang, "Effect of regeneration of liquid silk fibroin on its structure and characterization."

[13] M. Puerta, M. C. Arango, N. Jaramillo-Quiceno, C. Álvarez-López, and A. Restrepo-Osorio, "Influence of ethanol post-treatments on the properties of silk protein materials," *SN Appl. Sci.*, vol. 1, no. 11, pp. 1–7, Nov. 2019.

[14] Y. Zhang, F. Han, S. Fan, and Y. Zhang, "Low-power and tunable-performance biomemristor based on silk fibroin," *ACS Biomater. Sci. Eng.*, vol. 7, no. 7, pp. 3459–3468, Jul. 2021.

[15] S. Calamak, E. A. Aksoy, N. Ertas, C. Erdogdu, M. Sagiroglu, and K. Ulubayram, "Ag/silk fibroin nanofibers: Effect of fibroin morphology on Ag+ release and antibacterial activity," *Eur. Polym. J.*, vol. 67, pp. 99–112, Jun. 2015.

[16] A. S. Lammel, X. Hu, S. H. Park, D. L. Kaplan, and T. R. Scheibel, "Controlling silk fibroin particle features for drug delivery," *Biomaterials*, vol. 31, no. 16, pp. 4583–4591, Jun. 2010.

[17] H. Y. Wang, S. F. Zhou, M. Zhang, H. Da Wang, and Y. Q. Zhang, "The post-processing temperature or humidity can importantly control the secondary structure and characteristics of silk fibroin films," *J. Biomed. Mater. Res. - Part A*, vol. 110, no. 4, pp. 827–837, Apr. 2022.

[18] K. Yazawa, K. Ishida, H. Masunaga, T. Hikima, and K. Numata, "Influence of Water Content on the β-Sheet Formation, Thermal Stability, Water Removal, and Mechanical Properties of Silk Materials," *Biomacromolecules*, vol. 17, no. 3, pp. 1057–1066, Mar. 2016.

[19] C. Zhang, D. Song, Q. Lu, X. Hu, D. L. Kaplan, and H. Zhu, "Flexibility regeneration of silk fibroin in vitro.," *Biomacromolecules*, vol. 13, no. 7, pp. 2148–2153, 2012.

[20] M. Lovett, G. Eng, J. A. Kluge, C. Cannizzaro, G. Vunjak-Novakovic, and D. L. Kaplan, "Tubular silk scaffolds for small diameter vascular grafts," *Organogenesis*, vol. 6, no. 4, pp. 217–224, Oct. 2010.

[21] L. Wei *et al.*, "3D printing of silk fibroin-based hybrid scaffold treated with platelet rich plasma for bone tissue engineering," *Bioact. Mater.*, vol. 4, pp. 256–260, Dec. 2019.

[22] M. J. Rodriguez, T. A. Dixon, E. Cohen, W. Huang, F. G. Omenetto, and D. L. Kaplan, "3D freeform printing of silk fibroin," *Acta Biomater.*, vol. 71, pp. 379–387, Apr. 2018.

[23] S. Ghosh, S. T. Parker, X. Wang, D. L. Kaplan, and J. A. Lewis, "Direct-write assembly of microperiodic silk fibroin scaffolds for tissue engineering applications," *Adv. Funct. Mater.*, vol. 18, no. 13, pp. 1883–1889, Jul.

2008.

[24] X. Mu, J. K. Sahoo, P. Cebe, and D. L. Kaplan, "Photo-Crosslinked Silk Fibroin for 3D Printing," *Polym. 2020, Vol. 12, Page 2936*, vol. 12, no. 12, p. 2936, Dec. 2020.

[25] E. Casanova-Batlle, C. Santiago, A. J. Guerra, and J. Ciurana, "ESB2021," *Poster Sess. Biomater. Biofabrication, Poster Number PS2-01-014, B. Abstr. 31st Annu. Conf. Eur. Soc. Biomater. (ESB 2021), together with 43rd Annu. Congr. Iber. Soc. Biomech. a*, 2021.

[26] D. N. Rockwood, R. C. Preda, T. Yücel, X. Wang, M. L. Lovett, and D. L. Kaplan, "Materials fabrication from Bombyx mori silk fibroin," *Nat. Protoc.*, vol. 6, no. 10, pp. 1612–1631, Oct. 2011.

[27] L. S. Wray *et al.*, "Effect of Processing on Silk-Based Biomaterials: Reproducibility and Biocompatibility," *J. Biomed. Mater. Res. B. Appl. Biomater.*, vol. 99, no. 1, p. 89, Oct. 2011.

[28] Z. Liu, Y. Wan, H. Dou, and J. H. He, "Effect of Na2CO3 degumming concentration on LiBr-formic acid-silk fibroin solution properties," *Therm. Sci.*, vol. 20, no. 3, pp. 985–991, 2016.

[29] M. A. Koperska *et al.*, "Degradation markers of fibroin in silk through infrared spectroscopy," *Polym. Degrad. Stab.*, vol. 105, no. 1, pp. 185–196, Jul. 2014.

[30] J. Magoshi, Y. Magoshi, and S. Nakamura, "Physical properties and structure of silk. III. The glass transition and conformational changes of tussah silk fibroin," *J. Appl. Polym. Sci.*, vol. 21, no. 9, pp. 2405–2407, Sep. 1977.

[31] X. Hu *et al.*, "Regulation of silk material structure by temperature-controlled water vapor annealing," *Biomacromolecules*, vol. 12, no. 5, pp. 1686–1696, May 2011.

[32] A. Motta, L. Fambri, and C. Migliaresi, "Regenerated Silk Fibroin Films: Thermal and Dynamic Mechanical Analysis."

[33] D. N. Rockwood, R. C. Preda, T. Yücel, X. Wang, M. L. Lovett, and D. L. Kaplan, "Materials fabrication from Bombyx mori silk fibroin," *Nat. Protoc.*, vol. 6, no. 10, pp. 1612–1631, Oct. 2011.

[34] U. J. Kim, J. Park, C. Li, H. J. Jin, R. Valluzzi, and D. L. Kaplan, "Structure and properties of silk hydrogels," *Biomacromolecules*, vol. 5, no. 3, pp. 786–792, May 2004.

[35] B. P. Partlow, A. P. Tabatabai, G. G. Leisk, P. Cebe, D. L. Blair, and D. L. Kaplan, "Silk Fibroin Degradation Related to Rheological and Mechanical Properties," *Macromol. Biosci.*, vol. 16, no. 5, pp. 666–675, May 2016.

[36] R. L. Horan *et al.*, "In vitro degradation of silk fibroin," *Biomaterials*, vol. 26, no. 17, pp. 3385–3393, Jun. 2005.

[37] M. Samie *et al.*, "Aqueous Solution of a Basic Ionic Liquid: A Perspective Solvent for Extraction and Regeneration of Silk Powder from Bombyx mori Silk Cocoons," vol. 28, pp. 657–667, 2020.

[38] D. T. Pham, N. Saelim, and W. Tiyaboonchai, "Crosslinked fibroin nanoparticles using EDC or PEI for drug delivery: physicochemical properties, crystallinity and structure," *J. Mater. Sci.*, vol. 53, no. 20, pp. 14087–14103, Oct. 2018.

[39] S. Kaewpirom and S. Boonsang, "Influence of alcohol treatments on properties of silk-fibroin-based films for highly optically transparent coating applications," *RSC Adv.*, vol. 10, no. 27, pp. 15913–15923, Apr. 2020.

[40] M. Puerta, M. C. Arango, N. Jaramillo-Quiceno, C. Álvarez-López, and A. Restrepo-Osorio, "Influence of ethanol post-treatments on the properties of silk protein materials," *SN Appl. Sci.*, vol. 1, no. 11, pp. 1–7, Nov. 2019.

[41] J. Floor, B. Van Deursen, and E. Tempelman, "Tensile strength of 3D printed materials: Review and reassessment of test parameters," *Mater. Test.*, vol. 60, no. 7–8, pp. 679–686, Jul. 2018.

[42] T. Yucel, M. L. Lovett, and D. L. Kaplan, "Silk-based biomaterials for sustained drug delivery," *J. Control. Release*, vol. 190, pp. 381–397, Sep. 2014.

Characterization of direct ink write pure silk fibroin based on alcohol post-treatments

Enric Casanova-Batlle[a], Antonio J. Guerra[b], Joaquim Ciurana[a]

[a] Grup de Recerca d'Enginyeria Producte Procès i Producció, Universitat de Girona, Pic de Peguera 15, 17003, Girona, Spain.

[b] EURECAT, Centre Tecnològic de Catalunya, Plaça de la Ciència 2, 08243 Manresa, Spain

* Corresponding:

Email: quim.ciurana@udg.edu

Present address: [a] Grup de Recerca d'Enginyeria Producte Procès i Producció, Universitat de Girona, Pic de Peguera 15, 17003

Highlights

- Silk fibroin can be concentrated in an aqueous medium into a solution viscous enough to be 3D printed as an ink.
- Post-treatment of silk fibroin-based inks with alcohols improves their mechanical properties and catalyzes a water-insoluble product.
- The post treatment of silk fibroin with ethanol at 24 hours provides a good compromise between mechanical properties, flexibility and degradation in phosphate-buffered saline.

Enric Casanova-Batlle: Conceptualization, Methodology, Formal analysis, Investigation, Writing - Original Draft and Visualization.

Antonio J. Guerra: Conceptualization, Methodology, Validation, Writing - Review & Editing, Supervision and Project administration.

Joaquim Ciurana: Conceptualization, Methodology, Validation, Resources, Writing - Review & Editing, Supervision, Project administration and Funding acquisition

Declaration of interests

☒ The authors declare that they have no known competing financial interests or personal relationships that could have appeared to influence the work reported in this paper.

☐The authors declare the following financial interests/personal relationships which may be considered as potential competing interests: